Journal of Sound and Vibration (1997) **206**(3), 371–398

NON-COLLOCATED ADAPTIVE–PASSIVE VIBRATION CONTROL

C. Buhr, M. A. Franchek and R. J. Bernhard

Ray W. Herrick Laboratories, School of Mechanical Engineering, Purdue University, West Lafayette, IN 47907-1077, *U.S.A.*

(*Received* 24 *June* 1996, *and in final form* 20 *April* 1997)

Presented in this paper is the development of a control law for tuning a variable stiffness vibration absorber to attenuate single frequency excitation in a non-collocated situation. The control law is comprised of two distinct parts. First, a feedback controller is used to obtain a $\pm 90^\circ$ phase condition between the motion of the vibration absorber mass and the location of interest. Next, a feedback based tuning strategy is used to precisely tune the vibration absorber for performance maximization. The feedback based tuning is based on the classical feedback structure of a regulating system and is used to tune the absorber such that the accelerometer voltage resulting from the measurement of vibration of the point of interest is minimized. An experimental verification of this control law is shown.

1. INTRODUCTION

In many applications of vibration control, the sensor (at the point of interest for control) is collocated with the vibration control actuator [1–5]. Unfortunately, for some applications it is not possible to collocate the vibration control actuator at the location of interest. This complicates the control problem because the dynamics of the intervening structure between the control actuator and sensor plays a key role in the performance of the vibration control system.

Thus far, only active control methods have been developed for the non-collocated vibration control problem. For example, Bong *et al*. [6] used a H_∞ design technique to design a controller to reduce the effects of solar array vibrations on telescope pointing jitter for the Hubble Space Telescope. Balas and Doyle [7] used the structured singular value approach to design a controller for a large flexible space structure which has closely spaced, lightly damped modes. Yang and Mote [8] introduced a time delay in the feedback loop to compensate for the phase difference between the actuator and sensor. This time delay reduces the non-collocated vibration control problem to the collocated case. Long *et al*. [9] used a neural network based on forward dynamics and decentralized control to attenuate vibrations.

In contrast to active approaches, an adaptive–passive approach for the non-collocated vibration control problem is presented in this paper. Specifically, a robust control law that effectively tunes a vibration absorber to provide steady state vibration control of single frequency harmonic excitations is developed. Such single frequencies excitations occur in rotating and reciprocating machinery. The first part of this paper presents an investigation of the steady state dynamic behavior of a non-collocated passive vibration absorber. This dynamic analysis is followed by the development of a robust feedback based tuning algorithm for adaptive–passive vibration control. Finally, a verification of this control law is presented.

0022–460X/97/380371 + 28 $25.00/0/sv971098

2. DYNAMIC ANALYSIS OF NON-COLLOCATION

Presented in this section is the dynamic analysis of multi-degree-of-freedom lumped parameter vibrating systems with a non-collocated passive vibration absorber. The class of systems addressed, shown schematically in Figure 1, has N degrees of freedom (N-DOF) which are excited by a single frequency input and a passive vibration absorber attached to the Nth mass. Parameters of the vibration absorber are sought such that the steady amplitude of the ith mass, where $i \in (1, \ldots, N-1)$ is minimized. This analysis will first focus on a 3-DOF system to illustrate the steady state attenuation performance of a passive vibration absorber. The trends for the 3-DOF case will be generalized to systems with a higher number of degrees of freedom.

2.1. 3-DOF SYSTEM DYNAMIC ANALYSIS

The 3-DOF system with a vibration absorber is shown in Figure 2. The performance goal is to minimize the amplitude of the non-collocated point of interest, either $|x_1(t)|$ or $|x_2(t)|$, by tuning the variable spring stiffness of the vibration absorber given that the system parameters M_q, C_q, and K_q are fixed, where $q \in I_{+/4}$. The following dynamic analysis will first consider the special case with no damping in the intervening structure. Later, system damping will be addressed by building upon the results of the undamped case.

2.1.1. *Steady state attenuation of* $|x_2(t)|$

The transfer function relating the excitation force $F(s)$ to the displacement of M_2, $X_2(s)$, is

$$X_2(s)/F(s) = \frac{[C_2 s + K_2][M_3 m s^4 + (C_3 m + M_3 c + cm)s^3 + (M_3 k + K_3 m + C_3 c + km)s^2 + (K_3 c + C_3 k)s + K_3 k]}{D(s)}, \tag{1}$$

where $D(s)$ denotes the characteristic equation of the system.

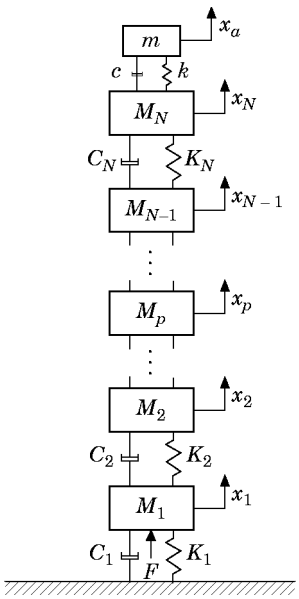

Figure 1. The N-DOF system model appended with a vibration absorber.

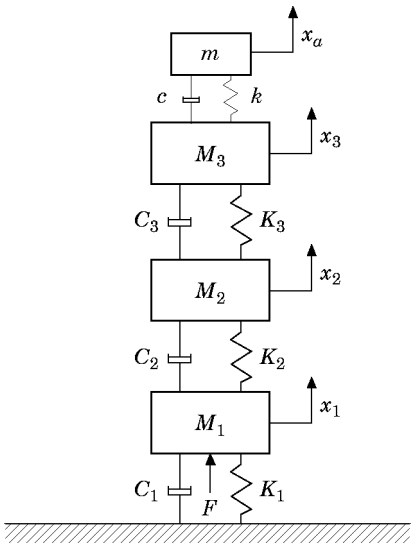

Figure 2. The 3-DOF system appended with a vibration absorber.

For complete steady state attenuation of $x_2(t)$ to occur, there must exist a real value k (vibration absorber spring stiffness) such that the numerator of equation (1) is zero for $s = j\omega$. The numerator of equation (1) is comprised of two polynomials in s. The first polynomial $(C_2 s + K_2)$ is not influenced by the vibration absorber spring stiffness k. The zeros of the remaining numerator polynomial can be rewritten in the form

$$1 + kG(s) = 1 + k \underbrace{\frac{(M_3 + m)s^2 + C_3 s + K_3}{M_3 m s^4 + (C_3 m + M_3 c + mc)s^3 + (K_3 m + C_3 c)s^2 + K_3 cs}}_{G(s)} = 0, \quad (2)$$

which resembles the classical root locus form, $1 + kG(s) = 0$ [10]. Thus, the dynamic analysis will proceed as a standard root locus analysis where the *system gain* to be varied is the vibration absorber spring stiffness k.

The zeros of equation (2) are the roots of the characteristic equation (CE) for the 2-DOF subsystem consisting of the intervening structure and vibration absorber. The transfer functions $X_i(s)/F(s) = N_i(s)/\alpha(s)$ and $X_a(s)/F(s) = N_a(s)/\alpha(s)$ relate the displacement of the ith mass and absorber mass to the excitation, respectively. The transfer function of the subsystem is $X_a(s)/X_i(s) = (X_a(s)/F(s))(F(s)/X_i(s)) = N_a(s)/N_i(s)$. Therefore the zeros of $X_i(s)/F(s)$ are roots of the CE of the subsystem $X_a(s)/X_i(s)$. This observation will provide physical insight in the analysis to follow.

2.1.1.1. *Analysis of $|x_2(t)|$ for undamped 3-DOF system*. For the case with no damping in the intervening structure and vibration absorber ($C_3 = c = 0$), equation (2) is

$$1 + k \frac{(M_3 + m)s^2 + K_3}{ms^2(M_3 s^2 + K_3)} = 1 + k \frac{(M_3 + m)(s^2 + \omega_A^2)}{mM_3 s^2(s^2 + \omega_B^2)} = 0. \quad (3)$$

The locus of transfer function zeros for equation (1) as a function of the vibration absorber spring stiffness k is shown in Figure 3. Because these zeros also correspond to the roots of the CE for the intervening structure and vibration absorber subsystem, each branch of

the locus of zeros along the positive imaginary axis correspond to the range for which the two natural frequencies of the subsystem can vary. Excitation frequencies for which the numerator of equation (1) is zero when $C_3 = c = 0$ correspond to the solutions where the *loci* intersect the imaginary axis. Consequently, the vibration absorber is appropriately tuned provided one of the two natural frequencies of the subsystem consisting of the intervening structure–vibration absorber assembly matches the excitation frequency. As shown in Figure 3, the tuned vibration absorber can achieve complete attenuation of $x_2(t)$ for any excitation frequency not contained within the range

$$\omega_A = \sqrt{\frac{K_3}{M_3 + m}} < \omega < \sqrt{\frac{K_3}{M_3}} = \omega_B . \tag{4}$$

In this frequency range, a natural frequency of the intervening structure–vibration absorber assembly does not exist. The first branch is upper bounded in frequency by the case when $k \to \infty$. Hence, with an infinite vibration absorber spring stiffness the two masses (m of the vibration absorber and M_3 of the intervening structure) act as a single collocated vibration absorber with mass $m + M_3$. The second branch is lower bounded in frequency when $k = 0$. Hence, there is no connection between m and M_3 and the intervening structure is acting as a vibration absorber. Complete attenuation of every other frequency not within the frequency range defined in equation (4) can be achieved using an appropriate real value for k. For excitation frequencies between ω_A and ω_B, performance is determined by the frequency responses of the system with $k = 0$ and $k = \infty$ as shown in Figure 4. The two branches of the *loci* also reveal that for a single vibration absorber stiffness, two excitation frequencies are attenuated simultaneously, although the two frequencies are not arbitrary.

2.1.1.2. *Analysis of $|x_2(t)|$ for damped 3-DOF system*. Using equation (2), the *loci* of zeros for equation (1) excluding $(C_2S + K_2)$ as a function of k for damped cases can be determined. For the first case $C_3 = 0$ and $c \neq 0$,

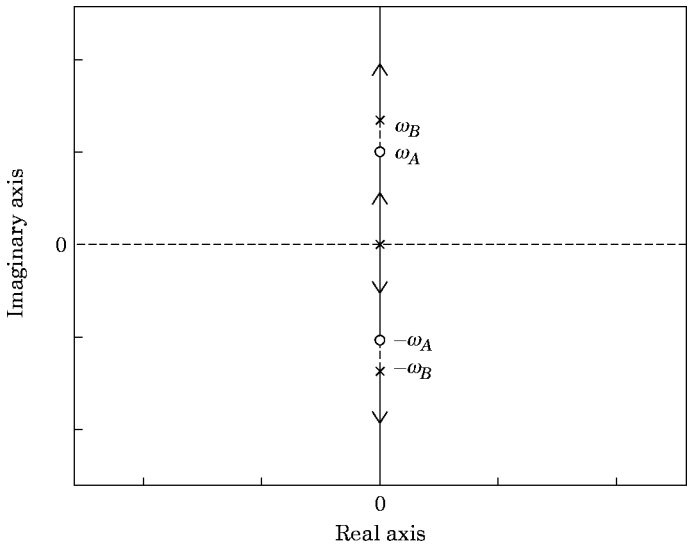

Figure 3. The locus of zeros for the case $C_3 = c = 0$. ×, poles of $G(s)$; ○, zeros of $G(s)$; $\omega_A = \sqrt{K_3/(M_3 + m)}$; $\omega_B = \sqrt{K_3/M_3}$.

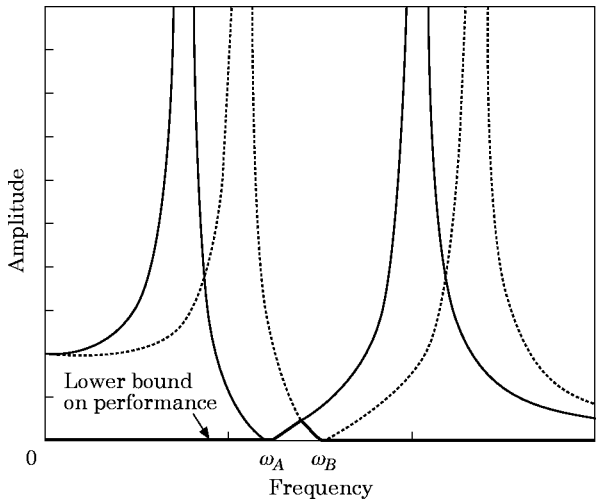

Figure 4. The lower performance bound for a non-collocated tuned vibration absorber. ——, $k = \infty$; · · · · ·, $k = 0$.

$$1 + k \underbrace{\frac{(M_3 + m)s^2 + K_3}{M_3 m s^4 + (M_3 c + mc)s^3 + (K_3 m)s^2 + K_3 cs}}_{G(s)} = 0. \tag{5}$$

The zeros of $G(s)$ in equation (5) remain purely imaginary. However, the pole in $G(s)$, which was originally at the origin for the undamped case, is now located on the negative real axis (Figure 5). The poles of $G(s)$ that were originally purely imaginary are now complex poles with negative real parts. Consequently, the *loci* of zeros for equation (1) do not intersect the imaginary axis except in the extreme case when $k \to \infty$. In this case, the two masses m and M_3 become one mass $(m + M_3)$ and behave as an undamped vibration absorber. Therefore, complete attenuation of $|x_2(t)|$ at steady state conditions can only be achieved in the extreme case at a specific excitation frequency.

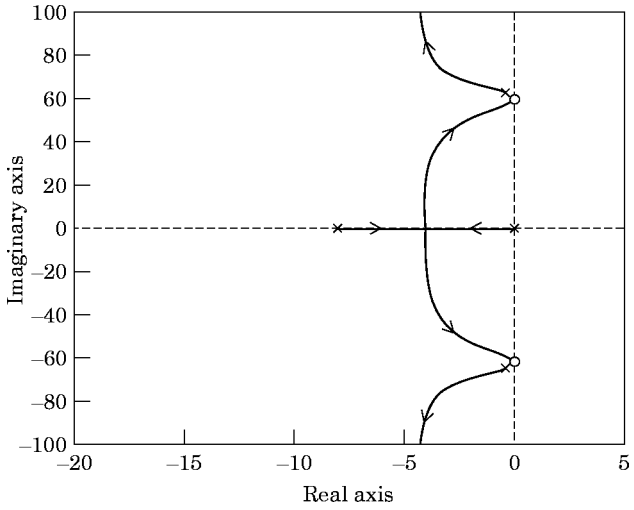

Figure 5. The locus of zeros for the case $C_3 = 0$, $c = 2\ Ns/m$. ×, poles of $G(s)$; ○, zeros of $G(s)$.

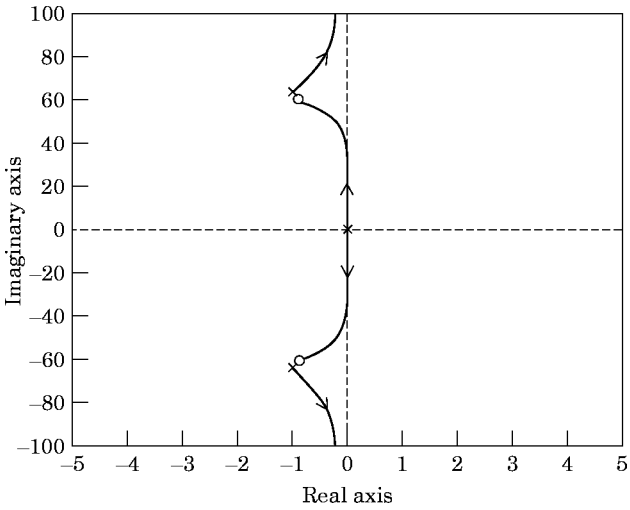

Figure 6. The locus of zeros for the case $C_3 = 5\ Ns/m$. $c = 0$. $\times$, Poles of $G(s)$; $\bigcirc$, zeros of $G(s)$.

Alternatively, for the case when $C_3 \neq 0$ and $c = 0$,

$$1 + k\frac{(M_3 + m)s^2 + C_3 s + K_3}{M_3 m s^4 + (C_3 m)s^3 + (K_3 m + C_3 c)s^2} = 0. \tag{6}$$

The zeros of $G(s)$ in equation (6) migrate from the imaginary axis into the complex plane with negative real parts. The two poles of $G(s)$ that were originally purely imaginary for the undamped case are now complex poles with negative real parts. The *loci* of zeros for equation (1) are shown in Figure 6. No purely imaginary zeros exist in this case. However, in the extreme case in which $C_3 \to \infty$, M_3 and M_2 behave as one mass $(M_2 + M_3)$ and the undamped vibration absorber is now collocated.

Hence, if damping exists in the intervening structure and/or the vibration absorber, complete attenuation of $|x_2(t)|$ cannot be realized. The performance goal of the vibration absorber in this case is then to minimize the magnitude of $|x_2(t)|$. To illustrate the effects of damping on performance, frequency responses for the system with parameters $M_1 = M_2 = M_3 = 2{\cdot}5$ kg, $K_1 = K_2 = K_3 = 10\ kN/m$, $m = 0{\cdot}25$ kg are shown in Figures 7–11. The performance for an undamped tuned vibration absorber for various values of system damping $C_q \neq 0$ are shown in Figures 7–10. The performance of a damped vibration absorber, $c \neq 0$ is shown in Figure 11. The solid line in these frequency responses are for the case where the absorber is not attached. The dashed line represents the maximum attainable attenuation of $|x_2(t)|$ with an optimally tuned vibration absorber. The attenuation performance which will serve as a benchmark is the case with the lowest value of C_q shown in Figure 7. Figures 8 and 9 reveal that the attenuation performance is not significantly sensitive to changes in the damping of the non-intervening structure except in a small frequency band at point B. In contrast, an increase in damping in either the intervening structure or absorber damping degrades performance as illustrated in Figures 10 and 11. Point A is the case in which the intervening structure alone behaves as a vibration absorber.

2.1.2. *Steady state attenuation of* $|x_1(t)|$

The non-collocated vibration control problem for control at $x_1(t)$ of the 3-DOF system is more complex due to an increase in the order of the intervening structure. The transfer

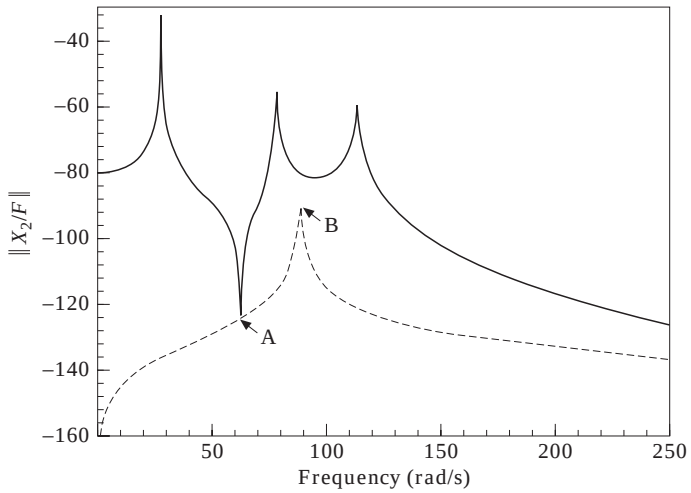

Figure 7. Frequency responses of X_2 for the 3-DOF system and the 3-DOF system appended with a tuned vibration absorber: $C_1 = 1\ Ns/m$, $C_2 = 1\ Ns/m$, $C_3 = 1\ Ns/m$, $c = 0$. —, response without absorber; ––, lower bound on response with tuned absorber.

function relating the displacement $X_1(s)$ with respect to the excitation force is

$$\begin{aligned} X_1(s)/F(s) = [&M_2M_3ms^6 + (M_2cm + C_2M_3m + C_3M_3m + M_2M_3c + M_2C_3m)s^5 \\ &+ (M_2C_3c + C_2M_3c + C_3cm + K_2M_3m + M_2M_3k + M_2km + C_3M_3c \\ &+ M_2K_3m + C_2cm + C_2C_3m + K_3M_3m)s^4 + (M_2C_3k + M_2K_3c \\ &+ C_2M_3k + K_2M_3c + C_2km + K_3cm + C_2C_3c + C_3M_3k + C_2K_3m \\ &+ K_2C_3m + C_3km + K_3M_3c + K_2cm)s^3 + (K_3M_3k + M_2K_3k \\ &+ K_3km + C_2C_3k + K_2M_3k + C_2K_3c + K_2km + K_2K_3m \\ &+ K_2C_3c)s^2 + (K_2C_3k + K_2K_3c + C_2K_3k)s + K_2K_3k]/D(s). \end{aligned} \tag{7}$$

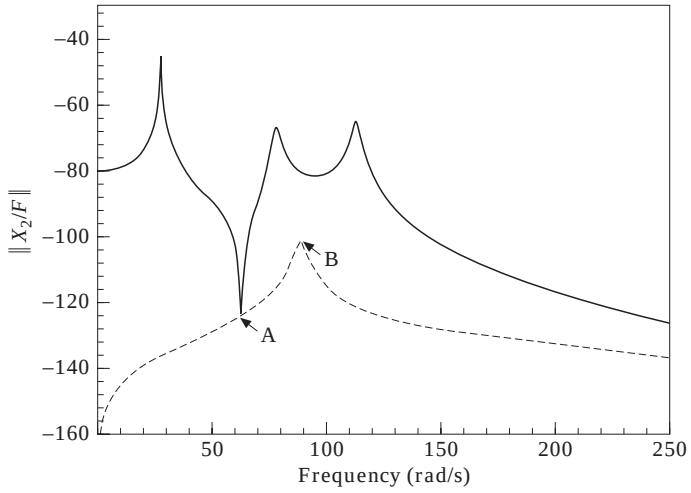

Figure 8. Frequency responses of X_2 for the 3-DOF system and the 3-DOF system appended with a tuned vibration absorber: $C_1 = 10\ Ns/m$, $C_2 = 1\ Ns/m$, $C_3 = 1\ Ns/m$, $c = 0$. —, response without absorber; ––, lower bound on response with tuned absorber.

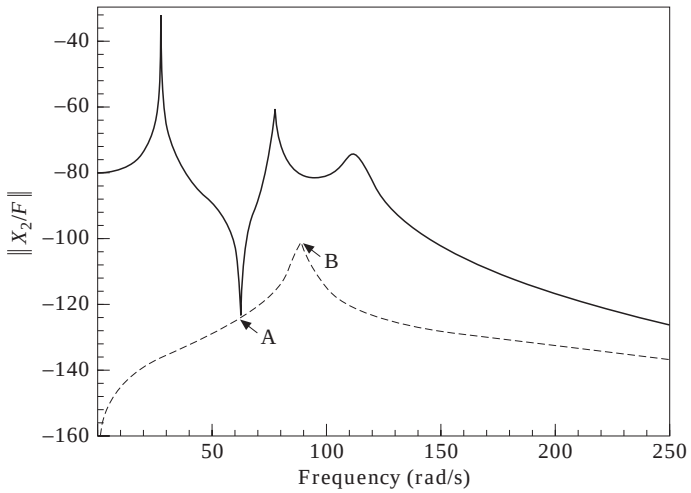

Figure 9. Frequency responses of X_2 for the 3-DOF system and the 3-DOF system appended with a tuned vibration absorber: $C_1 = 1\ Ns/m$, $C_2 = 10\ Ns/m$, $C_3 = 1\ Ns/m$, $c = 0$. —, response without absorber; ––, lower bound on response with tuned absorber.

The zeros of the numerator of equation (7) can be rewritten as

$$1 + k[(M_2m + M_2M_3)s^4 + (C_2m + C_2M_3 + C_3m + C_3M_3 + M_2C_3)s^3 + (K_3M_3 + K_3m + K_2m + C_2C_3 + M_2K_3 + K_2M_3)s^2 + (C_2K_3 + K_2C_3)s + K_2K_3]/D_1(s) = 0, \tag{8}$$

where

$$D_1(s) = M_2M_3ms^6 + (C_2M_3m + M_2C_3m + C_3M_3m + M_2M_3c + M_2cm)s^5 + (C_3M_3c + K_2M_3m + M_2K_3m + M_2C_3c + C_3cm + C_2M_3c + C_2C_3m + C_2cm + K_3M_3m)s^4 + (K_2cm + K_2M_3c + M_2K_3c + K_2C_3m + C_2K_3m + K_3cm + C_2C_3c + K_3M_3c)s^3 + (C_2K_3c + K_2K_3m + K_2C_3c)s^2 + K_2K_3cs.$$

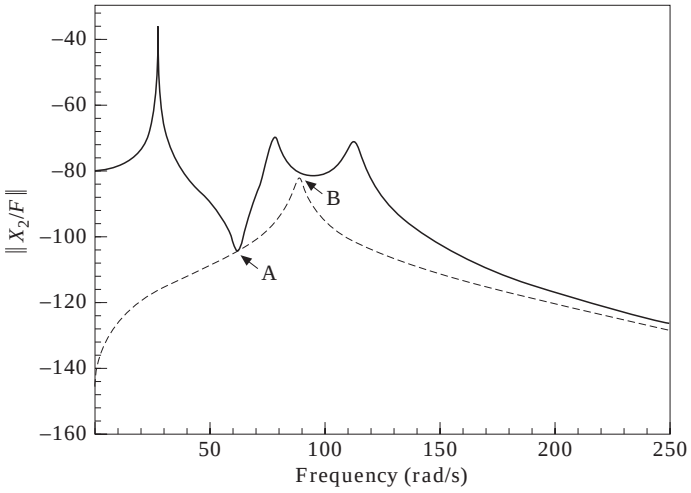

Figure 10. Frequency responses of X_2 for the 3-DOF system and the 3-DOF system appended with a tuned vibration absorber: $C_1 = 1\ Ns/m$, $C_2 = 1\ Ns/m$, $C_3 = 10\ Ns/m$, $c = 0$. —, response without absorber; ––, lower bound on response with tuned absorber.

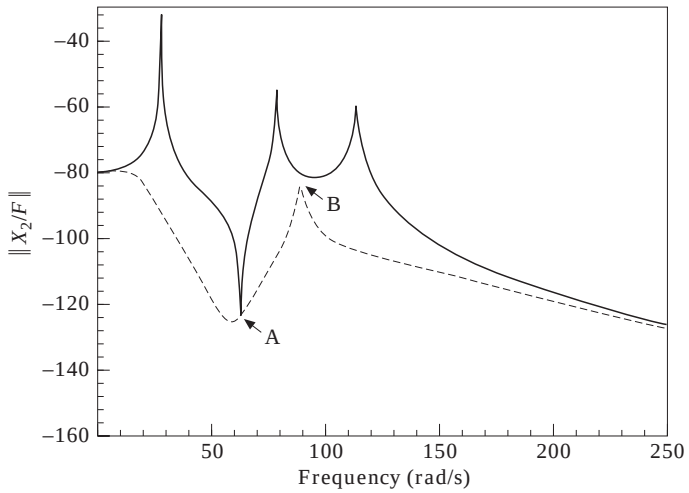

Figure 11. Frequency responses of X_2 for the 3-DOF system and the 3-DOF system appended with a tuned vibration absorber: $C_1 = 1\ Ns/m$, $C_2 = 1\ Ns/m$, $C_3 = 1\ Ns/m$, $c = 0{\cdot}1\ Ns/m$. —, response without absorber; ––, lower bound on response with tuned absorber.

The effect of the system parameters on the vibration absorber performance will be developed for both the undamped and damped case.

2.1.2.1. *Analysis of* $|x_1(t)|$ *for undamped 3-DOF system*. For the case of an undamped intervening structure and vibration absorber, equation (8) becomes

$$1 + k\frac{(M_2M_3 + M_2m)s^4 + (K_2m + M_2K_3 + K_3m + K_2M_3 + K_3M_3)s^2 + K_2K_3}{ms^2(M_2M_3s^4 + (K_2M_3 + K_3M_3 + M_2K_3)s^2 + K_2K_3)} = 0, \quad (9)$$

or, in factored form,

$$1 + k\frac{(M_2M_3 + M_2m)(s^2 + \omega_A^2)(s^2 + \omega_C^2)}{m(M_2M_3)s^2(s^2 + \omega_B^2)(s^2 + \omega_D^2)} = 0. \quad (10)$$

The locus of zeros is shown in Figure 12. Complete steady state attenuation of $|x_1(t)|$ is possible for the three frequency ranges $0 \leqslant \omega \leqslant \omega_A$, $\omega_B \leqslant \omega \leqslant \omega_C$ and $\omega_D \leqslant \omega \leqslant \infty$, where the locus of zeros coincides with the imaginary axis.

2.1.2.2. *Analysis of* $|x_1(t)|$ *for damped 3-DOF system*. The effects of damping in the intervening structure and vibration absorber on performance will be investigated in this section. Excluding the extreme cases, damping which causes the 3-DOF system to behave as a 2-DOF or a 1-DOF system, the performance will be analyzed based on the steady state minimization of $|x_1(t)|$. To illustrate the effects of damping on performance for an undamped tuned vibration absorber, frequency responses for the system with parameters $M_1 = M_2 = M_3 = 2{\cdot}5$ kg, $K_1 = K_2 = K_3 = 10$ kN/m, $m = 0{\cdot}25$ kg are given in Figures 13–16. The solid line in these frequency responses denotes the case when the absorber is not attached. The dashed line represents the maximum attainable attenuation of $|x_1(t)|$ with an optimally tuned vibration absorber. The attenuation performance plot of the system with least damping, which will serve as a benchmark, is shown in Figure 13. Points A and B represent the case in which the intervening structure acts as a vibration absorber. When the damping in the

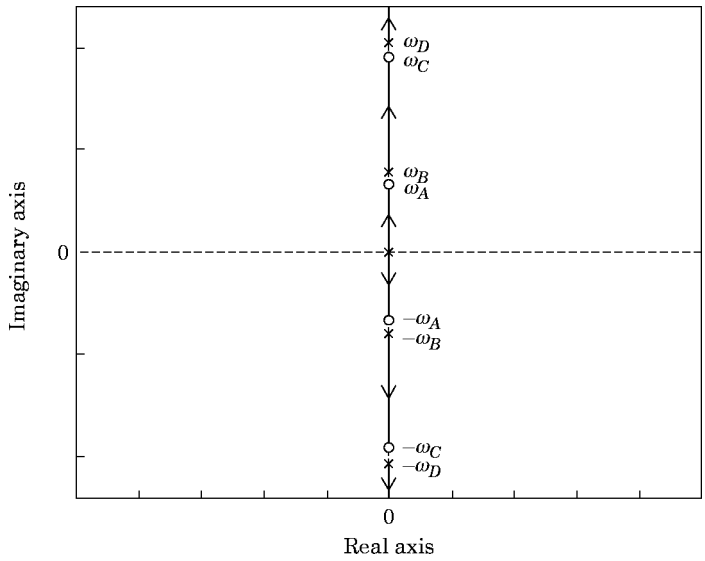

Figure 12. Locus of zeros for the case $C_2 = C_3 = c = 0$. $\times$, poles of $G(s)$; $\bigcirc$, zeros of $G(s)$.

non-intervening structure is increased, the performance does not change significantly as shown in Figure 14. However, when the damping in the intervening structure increases, the performance of the vibration absorber decreases, as shown in Figures 15 and 16. This emphasizes that the attenuation performance of the vibration absorber is contingent on the amount of damping in the intervening structure and vibration absorber.

2.2. GENERALIZATIONS

The analysis of the 3-DOF vibrating system shows the performance potential of a non-collocated passive vibration absorber. From this dynamic analysis, trends are revealed which can be generalized to an N-DOF system. Specifically, the zeros of the transfer

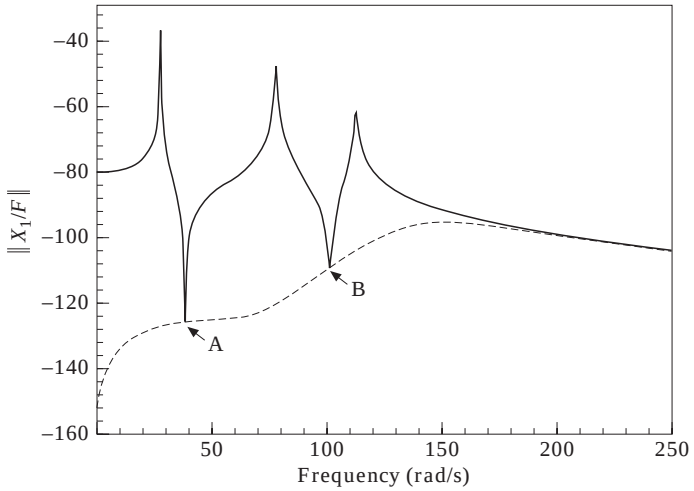

Figure 13. Frequency responses of X_1 for the 3-DOF system and the 3-DOF system appended with a tuned vibration absorber: $C_1 = 1\ Ns/m$, $C_2 = 1\ Ns/m$, $C_3 = 1\ Ns/m$, $c = 0$. —, response without absorber; ––, lower bound on response with tuned absorber.

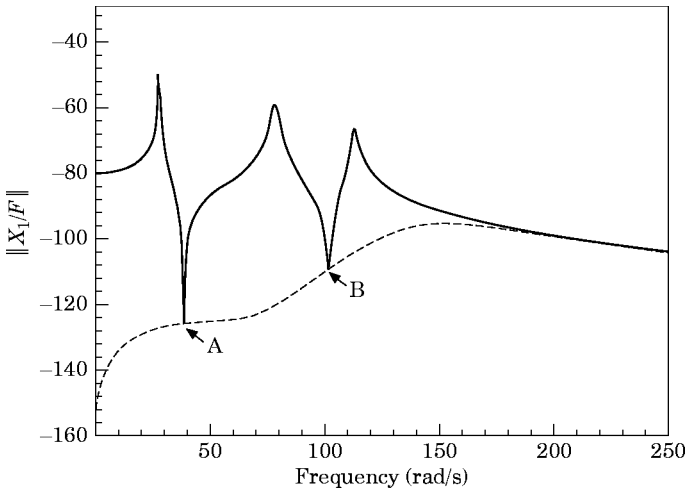

Figure 14. Frequency responses of X_1 for the 3-DOF system and the 3-DOF system appended with a tuned vibration absorber: $C_1 = 10\ Ns/m$, $C_2 = 1\ Ns/m$, $C_3 = 1\ Ns/m$, $c = 0$. —, response without absorber; ––, lower bound on response with tuned absorber.

function $X_i(s)/F(s)$ contain the characteristic equation of the subsystem consisting of both the intervening structure and absorber. For the undamped case, the amplitude of $|x_i(t)|$ can be completely attenuated when one of the natural frequencies of the intervening structure and vibration absorber subsystem matches the excitation frequency. Therefore, if there are L DOF in the intervening structure and vibration absorber subsystem, L different frequencies (although not arbitrary) can be attenuated for a given set of absorber parameters. Furthermore, damping in the intervening structure-vibration absorber assembly subsystem degrades attenuation performance. The analysis also demonstrated that performance curves associated with the vibration absorber intersect the frequency response of the original system without the vibration absorber at those frequencies where the intervening structure behaves as a vibration absorber. In the damped case, the

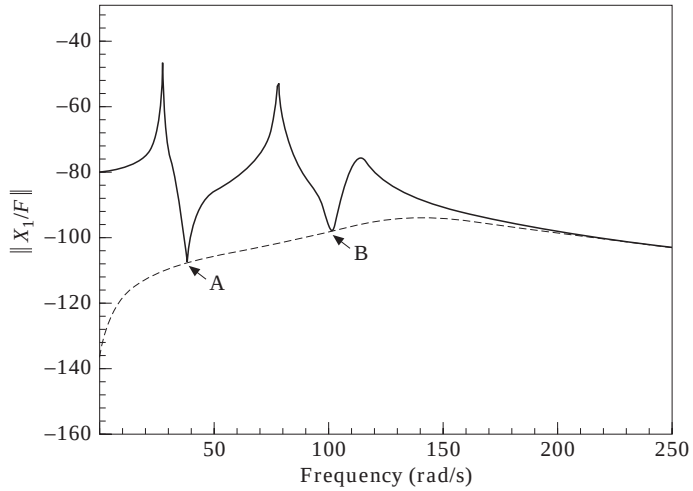

Figure 15. Frequency responses of X_1 for the 3-DOF system and the 3-DOF system appended with a tuned vibration absorber: $C_1 = 1\ Ns/m$, $C_2 = 10\ Ns/m$, $C_3 = 1\ Ns/m$, $c = 0$. —, response without absorber; ––, lower bound on response with tuned absorber.

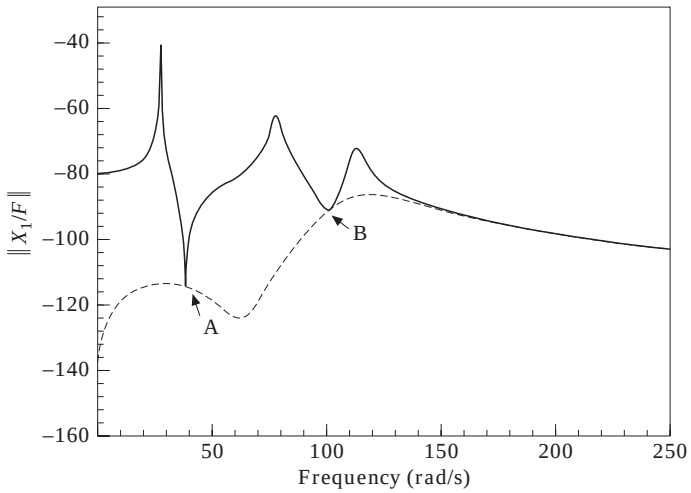

Figure 16. Frequency responses of X_1 for the 3-DOF system and the 3-DOF system appended with a tuned vibration absorber: $C_1 = 1\ Ns/m$, $C_2 = 1\ Ns/m$, $C_3 = 10\ Ns/m$, $c = 0$. —, response without absorber; ––, lower bound on response with tuned absorber.

attenuation performance of the vibration absorber is dependent on the frequency of interest and the amount of damping in the intervening structure and vibration absorber. In general, the vibration absorber is most effective when the system is being excited near a resonant frequency of the original system without the absorber attached.

3. CONTROL LAW DEVELOPMENT

Presented in this section is the development of a feedback based tuning algorithm for the non-collocated adaptive–passive vibration control problem. The objective of the algorithm is to tune a non-collocated vibration absorber such that the steady state amplitude at the point of interest is mimimized. The previous dynamic analysis revealed that complete steady state attenuation is only achievable (1) when damping is absent in both the vibration absorber and the intervening structure, and (2) when one of the natural frequencies of this subsystem consisting of the intervening structure–vibration absorber assembly matches the excitation frequency. Once damping is introduced, complete attenuation is not achievable. Hence the tuning and performance of the adaptive–passive vibration absorber becomes contingent upon the amount of damping. To develop the control law, a robust tuning algorithm will be developed first for the undamped case. This control law will then be modified so that it can be directly extended to the damped case.

3.1. ALGORITHM DEVELOPMENT FOR UNDAMPED CASE

The performance goal for tuning a non-collocated vibration absorber is to minimize the steady state amplitude of the ith mass, where $i \in I_{+/N}$. Consider the case when damping is absent in both the intervening structure and the vibration absorber, $C_q = c = 0$, where $q \in I_{(i+1)/(N+1)}$. To achieve precise tuning, the degree of attenuation performance and tuning direction must be identified. The degree of attenuation performance in this investigation will be determined by the amplitude of the ith mass which corresponds to the point of interest. The tuning direction will be determined using a phase condition which ensures that one of the natural frequencies of the intervening structure-vibration absorber assembly subsystem equals the excitation frequency. The subsystem has $N - i + 1$ degrees

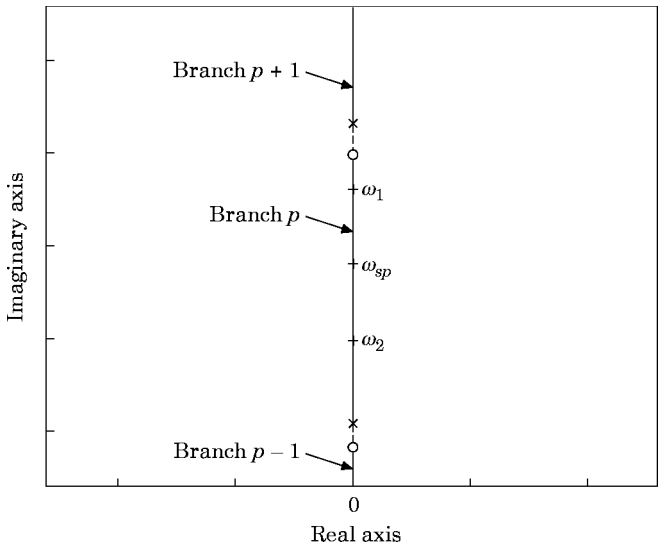

Figure 17. The pth branch of the locus of zeros for $X_i(s)/F(s)$.

of freedom and therefore $N-i+1$ natural frequencies. The ranges for these natural frequencies are bounded within the $N-i+1$ branches of the locus of zeros along the positive imaginary axis for the transfer function $X_i(s)/F(s)$ as the absorber spring stiffness is varied from 0 to ∞. Tuning information will be extracted from the locus of zeros for $X_i(s)/F(s)$. The pth branch of the locus, where ω_{sp} is the pth natural frequency of the subsystem, is illustrated in Figure 17. If the excitation frequency is $\omega = \omega_1 > \omega_{sp}$, the spring stiffness of the vibration absorber must be increased such that ω_{sp} equals ω_1. For the case $\omega = \omega_2 < \omega_{sp}$, the spring stiffness of the vibration absorber must be decreased such that ω_{sp} equals ω_2. A comparison between the excitation frequency and a natural frequency of the subsystem can be used to identify the required tuning direction. A realization of this comparison can be determined based on the phase difference between $x_a(t)$ and $x_i(t)$.

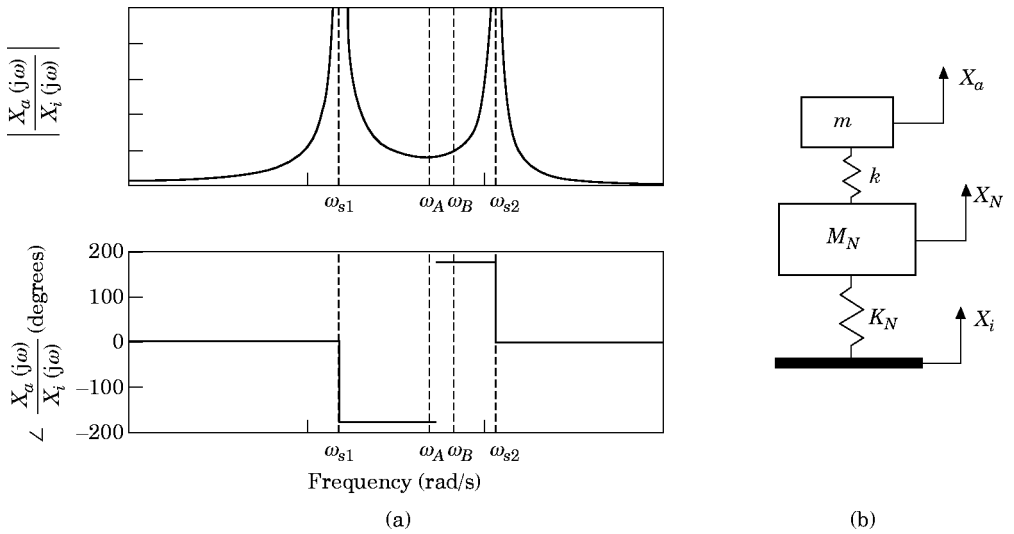

Figure 18. The frequency response (a) for a 2-DOF subsystem (b).

TABLE 1

Tuning direction

p	ω	$\angle \frac{X_a}{F} - \angle \frac{X_i}{F}$ (degrees)	k
1	$\omega < \omega_{s1}$	> -90	$\downarrow$
	$\omega > \omega_{s1}$	< -90	$\uparrow$
2	$\omega < \omega_{s2}$	$> +90$	$\downarrow$
	$\omega > \omega_{s2}$	$< +90$	$\uparrow$
Odd	$\omega < \omega_{sp}$	> -90	$\downarrow$
	$\omega > \omega_{sp}$	< -90	$\uparrow$
Even	$\omega < \omega_{sp}$	$> +90$	$\downarrow$
	$\omega > \omega_{sp}$	$< +90$	$\uparrow$

Shown in Figure 18 is a representative frequency response of the vibration absorber displacement $x_a(t)$ for a 2-DOF intervening structure–vibration absorber assembly subsystem $(N - i + 1) = 2$. The natural frequencies of the subsystem are labeled as ω_{sp} where $p = 1, 2$. When the excitation frequency is within the frequency range of the pth branch of the locus of zeros for the subsystem, the tuning relationship requires $\omega_{sp} = \omega$. For the 3-DOF subsystem (refer to Figure 18) when $0 < \omega < \omega_A$, the tuning condition is $\omega_{s1} = \omega$ and when $\omega_B < \omega < \infty$ the tuning requirement is $\omega_{s2} = \omega$. For the frequency interval $\omega_A < \omega < \omega_B$, the range of natural frequencies for the intervening structure–vibration absorber assembly is not able to be matched to the excitation frequency. Thus an absorber spring stiffness does not exist such that complete vibration attenuation can be achieved.

The phase information from the frequency response will be used to establish the required tuning direction for ω_{sp}. For instance, if ω is in the frequency range $(0, \omega_A)$ and $\omega < \omega_{s1}$, then the phase of the absorber for the subsystem is less than -90° and the absorber spring stiffness should be decreased. Various conditions for the different scenarios are tabulated in Table 1. The advantage of using the phase difference between $x_a(t)$ and $x_i(t)$ to establish the tuning direction is the robustness of this approach to system parameters (i.e., M's and K's) and to aging.

Determination of the phase between $x_a(t)$ and $x_i(t)$ can be realized with two accelerometers or other motion sensors (one attached to the mass of the vibration absorber and the other attached to the ith mass) and a synchronous demodulator. The synchronous demodulator (SD) is a device that has two inputs and one output. The operation of the SD is as follows: when input signal 1 crosses zero, integration of input signal 2 begins. Another zero crossing of input signal 1 terminates the integration and the value from this integration is the output of the synchronous demodulator. When both input signals to the synchronous demodulator are sinusoids of the same frequency, the synchronous demodulator can be used to determine the relative phase between the two input signals about $\pm 90^\circ$. Illustrated in Figures 19 and 20 is the operation of the synchronous demodulator for two cases. The signs of the output for the synchronous demodulator are tabulated in Table 2. The sign of the synchronous demodulator output indicates tuning direction provided that it is known in which branch of the locus of zeros the excitation frequency is contained. Two accelerometers and a synchronous demodulator will provide

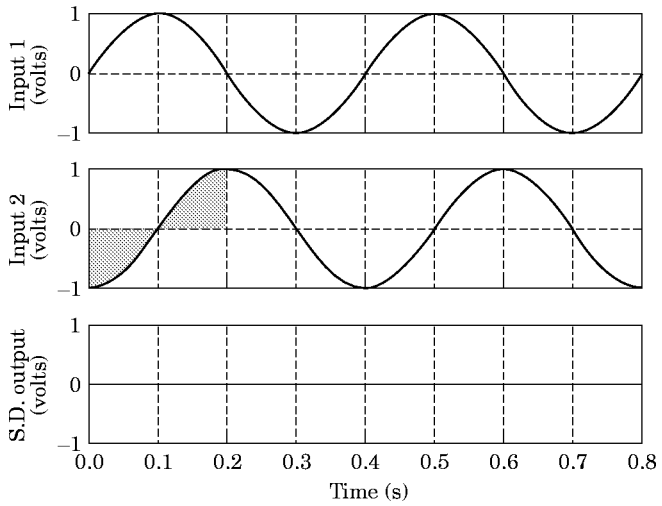

Figure 19. An example of a synchronous demodulator when input signal 2 lags input signal 1 by 90°.

the necessary information for tuning direction. A schematic of this configuration is shown in Figure 21.

3.2. ALGORITHM DEVELOPMENT FOR DAMPED CASE

A robust control algorithm for the precise tuning of a vibration absorber when damping is not present in the intervening structure–vibration absorber assembly is developed in the previous section. However, when damping exists in the intervening structure, this tuning scheme may need to be modified. In this section, a robust tuning algorithm is developed that extends the previous tuning scheme to a more general class of systems having damping in the intervening structure.

The precise tuning of the vibration absorber for the damped case is contingent on the amount of damping in the system which complicates the tuning process. Consequently, it is necessary to place restrictions on the class of systems addressed by the tuning control

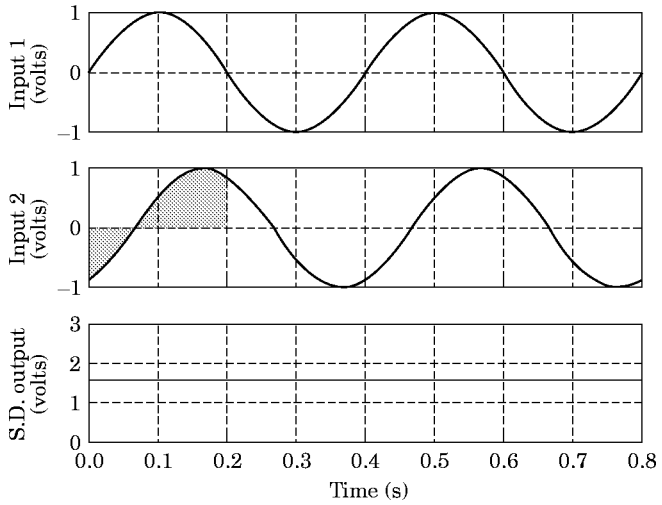

Figure 20. An example of a synchronous demodulator when input signal 2 lags input signal 1 by 60°.

TABLE 2

Output sign of synchronous demodulator

$\phi = \angle(\text{input}_1) - \angle(\text{input}_2)$	Synchronous demodulator output
$\phi = 90^\circ$	Zero
$\phi = -90^\circ$	Zero
$-90^\circ < \phi < 90^\circ$	Positive
$90^\circ < \phi < 270^\circ$	Negative

law. Damping causes the phase shift associated with each pole and zero to occur over a larger frequency range about the corresponding break frequencies. This, as well as closely spaced modes, can cause significant phase (modal) overlap which may distort the phase information between $x_a(t)$ and $x_i(t)$ such that tuning direction cannot be based solely on phase difference. The class of systems to be considered are lightly damped systems without closely spaced modes such that significant phase (modal) overlap does not occur. This class of problems is still relatively large, particularly at low frequencies for structures.

Shown in Figure 22 is a representative frequency response which illustrates the performance and tuning requirement for a 2-DOF system appended with a vibration absorber where $x_1(t)$ is to be minimized. This plot shows the phase relation between $x_a(t)$ and $x_1(t)$ as a function of frequency. At low frequencies the tuning requirement is similar to the tuning requirement for the undamped case. At higher frequencies the phase difference decreases. Similar trends can be developed for the 3-DOF system with a vibration absorber when either $x_1(t)$ or $x_2(t)$ is considered for attenuation, as shown in Figures 23 and 24, respectively.

These trends in the phase relationship between $x_a(t)$ and $x_i(t)$ can provide the necessary information required for extending the tuning algorithm of the undamped case to a tuning algorithm for the damped case. Consider the frequency response of $X_1(s)/F(s)$ shown in Figure 22 for the 2-DOF system, where the desired attenuation is

$$\left\| \frac{X_1(\mathrm{j}\omega)}{F(\mathrm{j}\omega)} \right\| \leqslant \delta.$$

As shown in the phase information, at low frequencies the desired performance is obtained using the tuning method for the undamped case. For higher frequencies, the solution developed for the undamped tuning method does not tune the absorber to the optimal conditions. Although the undamped tuning method does not result in optimal tuning at high frequencies, it provides a starting point for which a feedback based tuning approach can be developed. The phase difference between $x_a(t)$ and $x_i(t)$ achieved using the undamped system condition provides the necessary tuning direction. To decrease the phase difference between $x_a(t)$ and $x_i(t)$, feedback based tuning [1] is used to increase the absorber spring stiffness (increasing the break frequencies of the zeros for $X_i(s)/F(s)$) until the desired performance level of $|x_1(t)| \leqslant \hat{\delta}$ is achieved, where $\hat{\delta}$ is the time domain representation of δ.

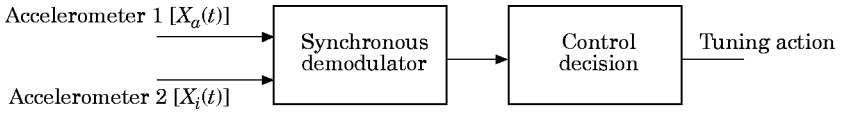

Figure 21. A schematic of an undamped tuning scheme.

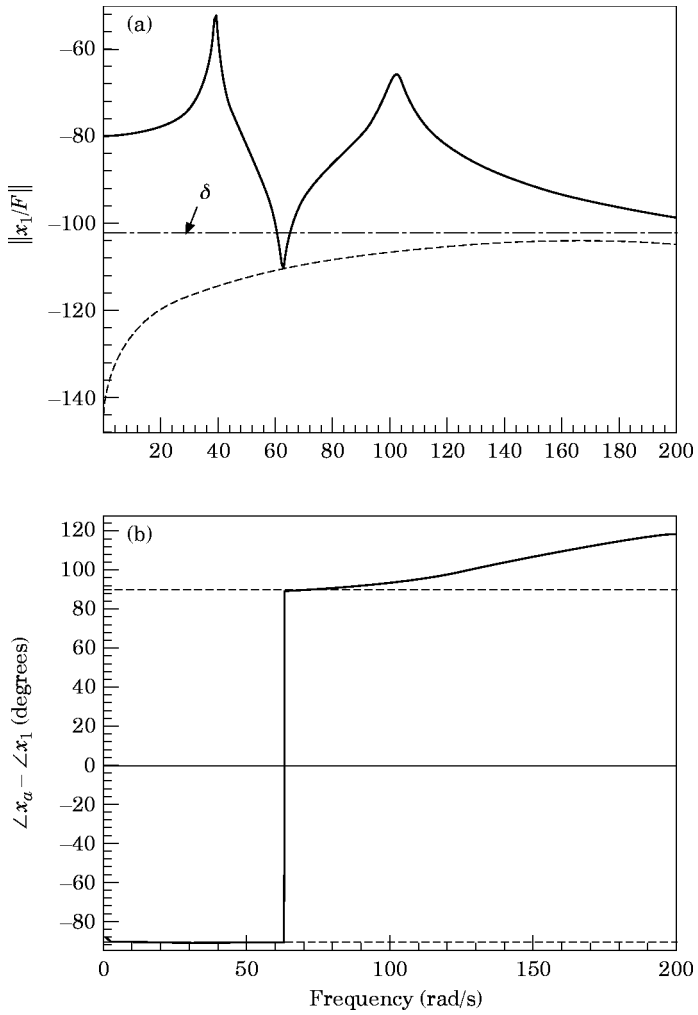

Figure 22. (a) The performance and (b) the tuning condition for $x_1(t)$ of the 2-DOF system appended with a vibration absorber: $M_1 = M_2 = 2{\cdot}5$ kg, $K_1 = K_2 = 10\,kN/m$, $C_1 = C_2 = 5\,Ns/m$, $m = 0.25$ kg, $c = 0$.

The tuning algorithm which extends the undamped tuning method to make it applicable to systems with damping is presented in Figure 25. For stage 1, the algorithm is identical to the undamped case. Once the vibration absorber is tuned based on the undamped case (i.e., the output of the synchronous demodulator signal is driven to zero), the amplitude of $x_i(t)$ is compared with a achievable desired level $\hat{\delta}$. If the $|x_i(t)| > \hat{\delta}$, the controller begins increasing the absorber spring stiffness until $|x_i(t)| \leqslant \hat{\delta}$. The absorber spring stiffness then remains constant until $|x_i(t)| > \hat{\delta}$ (due to environmental changes) at which time the tuning control law begins the tuning process again.

The phase relation between $x_a(t)$ and $x_i(t)$ and the amplitude of $x_i(t)$ are the two necessary pieces of system information required such that the tuning algorithm will initiate the appropriate action. Using two accelerometers, one attached to absorber mass and the other attached to the ith mass, the synchronous demodulator can be used to provide the phase relationship between $x_a(t)$ and $x_i(t)$. The amplitude of $x_i(t)$ can be obtained by passing the accelerometer signal representing $x_i(t)$ through a rectifier and capacitor. This

will provide a DC voltage (V_{RC}) representation of the amplitude of vibration. A schematic of this configuration is shown in Figure 26.

The choice of $\hat{\delta}$ is significant. If $\hat{\delta}$ is chosen to be too small, the absorber spring stiffness will not converge to a value in stage two of the controller. If $\hat{\delta}$ is chosen to be too large, the performance of the absorber will not be maximized. An experimental approach can be used to choose $\hat{\delta}$. By implementing the controller on the system with $\hat{\delta}$ set to zero, an achievable level of performance can be determined from the time history of V_{RC}. From this time history, an appropriate value for $\hat{\delta}$ can be chosen.

4. EXPERIMENTAL AND SIMULATION RESULTS

The verification of the robust control tuning algorithm is presented in this section. First, experimental verification of the tuning control algorithm is performed on a scaled model building appended with a variable stiffness vibration absorber. The scaled model building

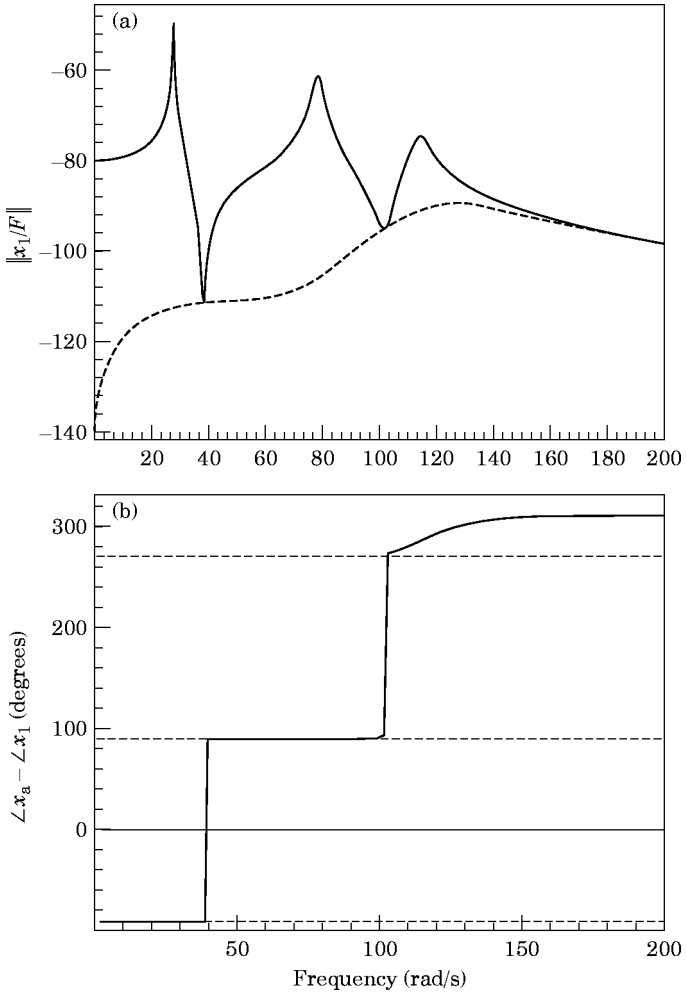

Figure 23. (a) The performance and (b) the tuning condition for $x_1(t)$ of the 3-DOF system appended with a vibration absorber: $M_1 = M_2 = M_3 = 2{\cdot}5$ kg, $K_1 = K_2 = K_3 = 10kN/m$, $C_1 = C_2 = C_3 = 5$ Ns/m, $m = 0{\cdot}25$ kg, $c = 0$.

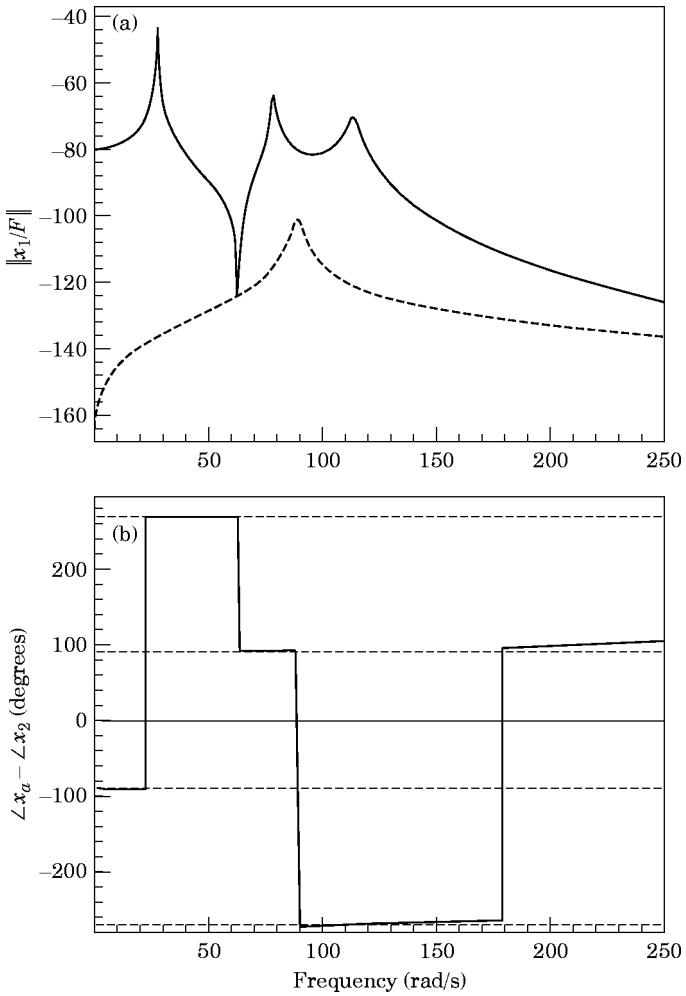

Figure 24. (a) The performance and (b) the tuning condition for $x_2(t)$ of the 3-DOF system appended with a vibration absorber: $M_1 = M_2 = M_3 = 2{\cdot}5$ kg, $K_1 = K_2 = K_3 = 10\,kN/m$, $C_1 = C_2 = 5\,Ns/m$, $C_3 = 1\,Ns/m$, $m = 0.25$ kg, $c = 0$.

is used as an abstract example for illustrative purposes. Due to the limited frequency range obtainable by the vibration absorber, it is not possible experimentally to verify the control algorithm at frequencies corresponding to the second mode of the building and above. Therefore, a virtual 3-DOF system (software system) implemented in real time will be used so that the supporting control hardware used in the experimental portion can be used for the verification. A detailed description of the experimental facility, the implementation of the tuning scheme, and the experimental results will be presented.

4.1. EXPERIMENTAL TEST FACILITY

The experimental test facility is shown schematically in Figure 27. The structure is a four-story model building which can be represented as a 4-DOF lumped parameter system. The bottom of the structure is rigidly attached to an APS Electro-Seis long stroke shaker which is driven using single frequency excitation. The excitation signal to the shaker table is generated by a Wavetek Model 75 digital signal generator. The amplifier used to drive

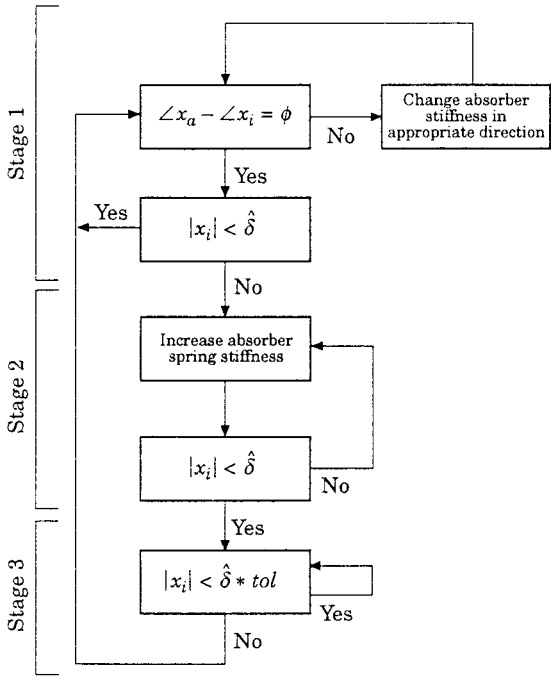

Figure 25. The tuning algorithm flow diagram.

the shaker is a QSC audio power amplifier. The accelerometers are PCB model 302A and have a sensitivity of 10 mV/g. The variable stiffness vibration absorber is appended to the top of the structure. Accelerometers are mounted on the vibration absorber mass and the floor of interest, and serve as feedback sensors for the controller.

A schematic of the variable stiffness vibration absorber is shown in Figure 28. The vibration absorber is supported by a base and two end plates. A guide rod is attached to the end plates and serves as a guide for the cylindrical mass which rides on a linear bearing. The vibration absorber is tunable. The DC motor and gearing are used to change the absorber spring stiffness by rotating the spring through the collar changing the number of active spring coils.

4.2. CONTROLLER IMPLEMENTATION

The adaptive–passive tuning algorithm is implemented on a Compaq 486-66 computer using Real Time Workshop, a toolbox produced by Math Works. A schematic for the control system is shown in Figure 29. The two accelerometers signals are used as the inputs

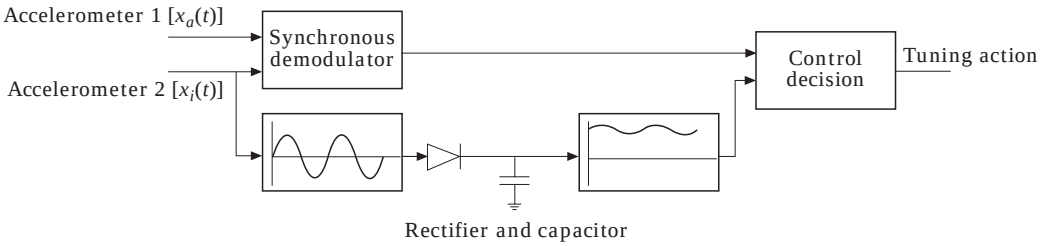

Figure 26. A schematic of the damped tuning scheme.

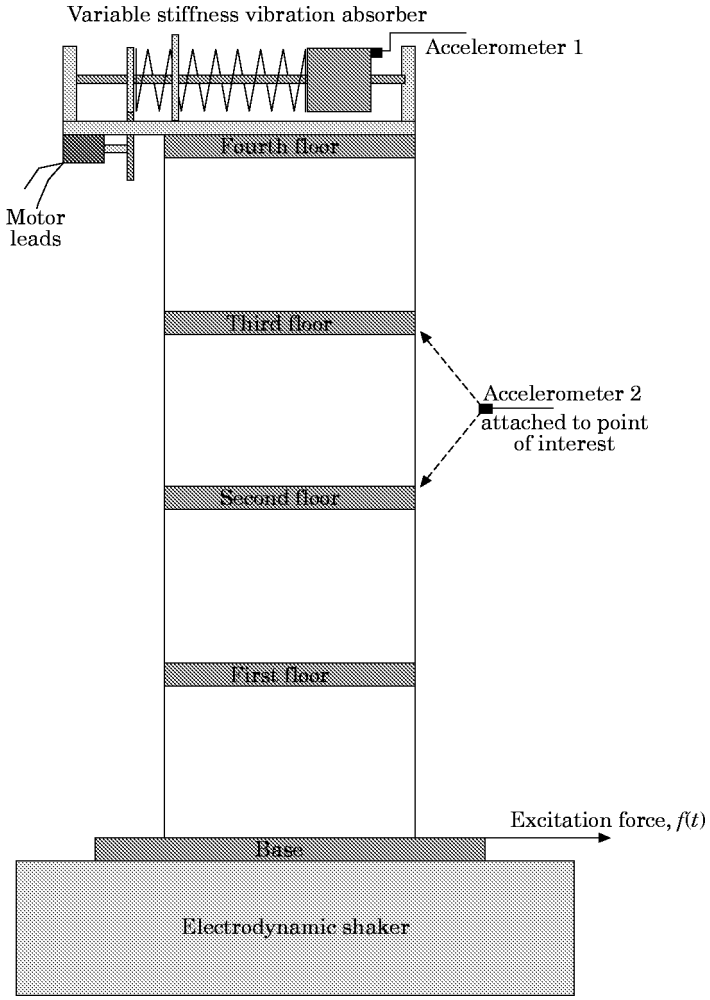

Figure 27. The shaker and 4-DOF building appended with a vibration absorber.

and the DC motor voltage, which drives the variable stiffness vibration absorber, is the output.

The accelerometer signals are passed through standard PCB amplifiers and sent to a band-pass filtering network. These cascaded high pass and low pass Wavetek filters remove both the high frequency signal noise and the DC offset from the two accelerometer signals. To preserve the relative phase between the two signals, the filters are identical. Removal of the DC offset is necessary for the triggering operation of the synchronous demodulator. The rectifier and capacitor circuit is used to provide a DC representation of the amplitude of vibration. Both the DC outputs from the synchronous demodulator and the rectifier/capacitor circuit are interfaced with an open architecture control system using Real Time Workshop (RTW) and Keithley data acquisition boards. The control law is developed in RTW. A dead zone in the control law is used to reduce chatter. The control algorithm processes the signals according to the flowchart in Figure 25. The appropriate control action from this algorithm is sent through a saturation element to limit the maximum voltage sent from the D/A board. This signal is then amplified with a current driver and sent to the DC motor to change the spring stiffness of the vibration absorber.

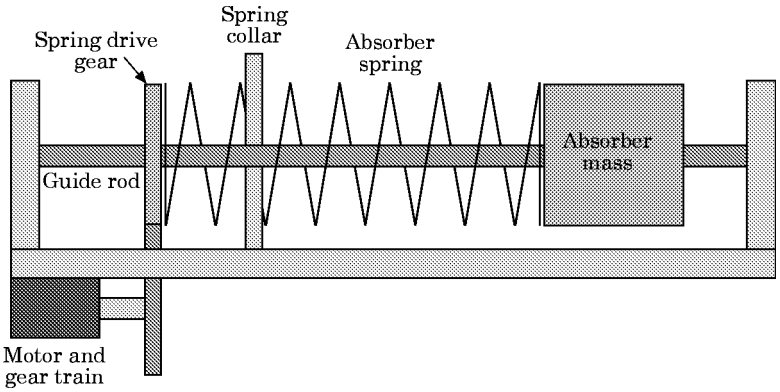

Figure 28. The variable stiffness vibration absorber.

4.3. EXPERIMENTAL RESULTS

Two tests were performed using the 4-DOF structure appended with a vibration absorber. The first test is concerned with the vibration attenuation of the third floor. Therefore, accelerometer 2 is mounted to the third floor. The second test is concerned with the vibration attenuation of the second floor. In each test, the vibration absorber is initially mistuned. When the control algorithm has tuned the vibration absorber, the excitation frequency is changed to illustrate robustness.

For each test, two sets of transient responses are shown. The first set consists of three transient plots. The first plot contains the output of the rectifier and capacitor circuit (V_{RC}). This voltage provides a DC representation of the amplitude of vibration for the location of interest. The second plot shows the stage of operation for the controller algorithm. During the first stage of operation, the vibration absorber is tuned such that the synchronous demodulator signal is zero. During the second stage, the absorber spring stiffness is increased such that the amplitude of vibration at the point of interest is attenuated within a prespecified tolerance ($\hat{\delta}$). During the third stage, the attenuation performance is achieved, namely $\hat{\delta} \geqslant V_{RC}$, and the controller simply monitors performance. The output of the synchronous demodulator (V_{SD}) is shown in the third transient plot. The performance of the adaptive–passive vibration absorber will be illustrated in the second set of figures. These transient responses contain the output responses of the 4-DOF structure both with and without the vibration absorber appended.

4.3.1. *Attenuation of the third floor*

Initially, the structure is excited at a frequency of 6·5 Hz. The tuning algorithm is activated at $t = 5$ s. At $t = 30$ s, the excitation frequency is changed to 6 Hz. The control algorithm parameters ϕ and $\hat{\delta}$ are contingent upon the excitation and system parameters. For this test, these parameters are $\phi = -90^{\circ}$, $\hat{\delta} = 0{\cdot}8$ and $tol = 1{\cdot}2$. The results of the test

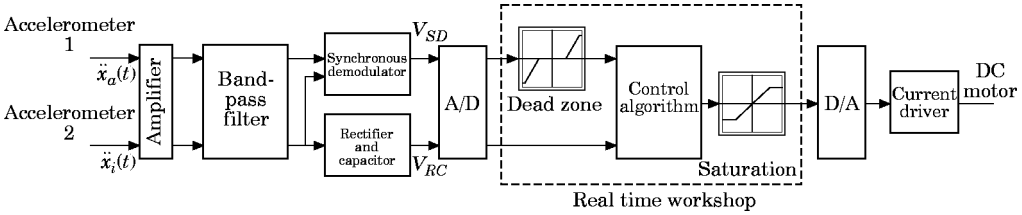

Figure 29. Implementation of the control scheme.

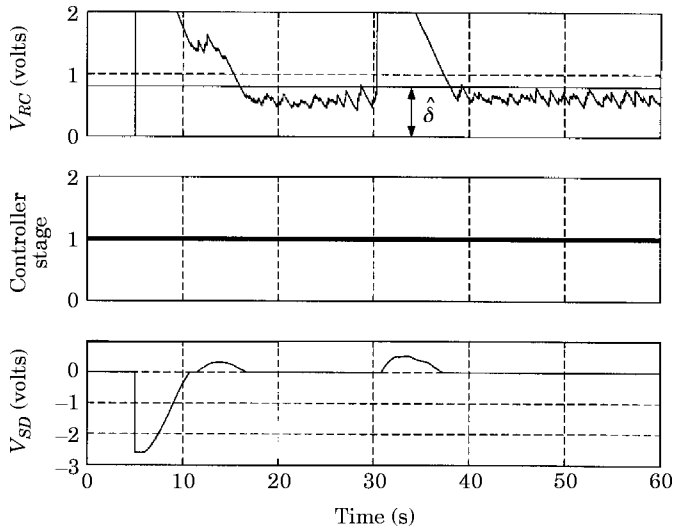

Figure 30. Experimental results with the third floor as the point of interest.

are shown in Figures 30 and 31. The control process for this test is shown in Figure 30. Initially, the controller is in the first stage of operation. At approximately $t = 17$ s, the output of the synchronous demodulator reaches zero. Since V_{RC} is less than $\hat{\delta}$, the controller remains in the first stage. At $t = 30$ s, the excitation frequency changes and the algorithm begins to retune the vibration absorber to drive V_{SD} to zero.

The performance of the adaptive–passive vibration absorber is illustrated in Figure 31 by comparing the responses of the third floor for the 4-DOF system both with and without the adaptive vibration absorber. At steady state, the tuned vibration absorber achieves a 24·2 dB and 24·3 dB reduction in the amplitude of filtered accelerometer signal of the third floor for the excitation frequencies of 6·5 Hz and 6 Hz respectively.

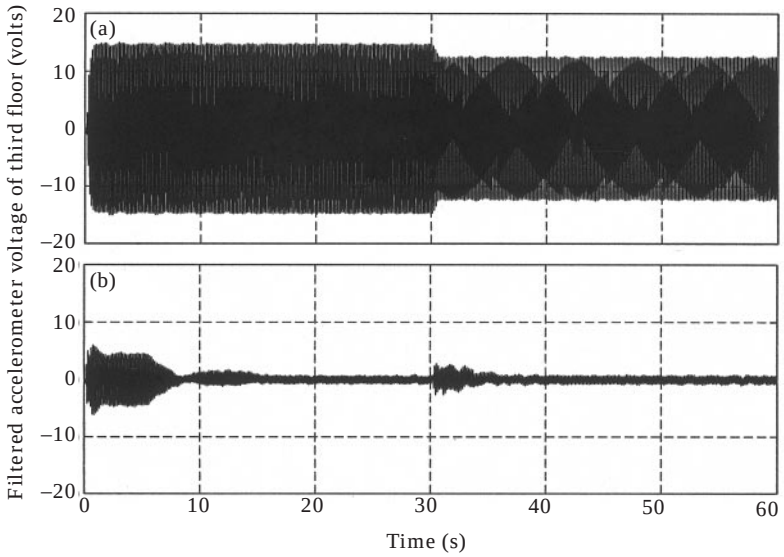

Figure 31. The performance of the adaptive–passive vibration absorber with the third floor as the point of interest: (a) response without vibration absorber appended; (b) response with vibration absorber appended.

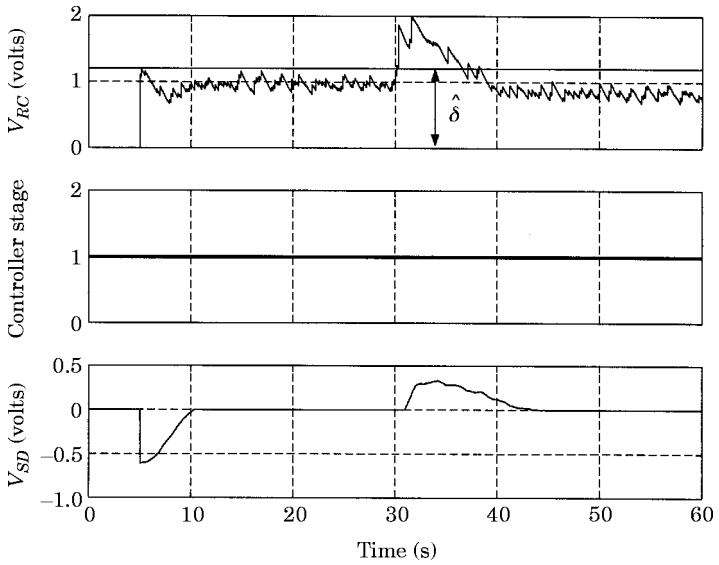

Figure 32. Experimental results with the second floor as the point of interest.

4.3.2. *Attenuation of the second floor*

For the second test, the structure is initially excited at a frequency of 6 Hz. Again, the tuning algorithm is activated at $t = 5$ s. At $t = 30$ s, the excitation frequency is changed to 5·6 Hz. For this test, the control algorithm parameters are $\phi = -90^{\circ}$, $\hat{\delta} = 1{\cdot}2$ and $tol = 1{\cdot}2$. The results of the test are shown in Figures 32 and 33. The control process for this test, shown in Figure 32, is similar to the previous test. The controller stays in the first stage for the entire test. The performance of the adaptive–passive vibration absorber

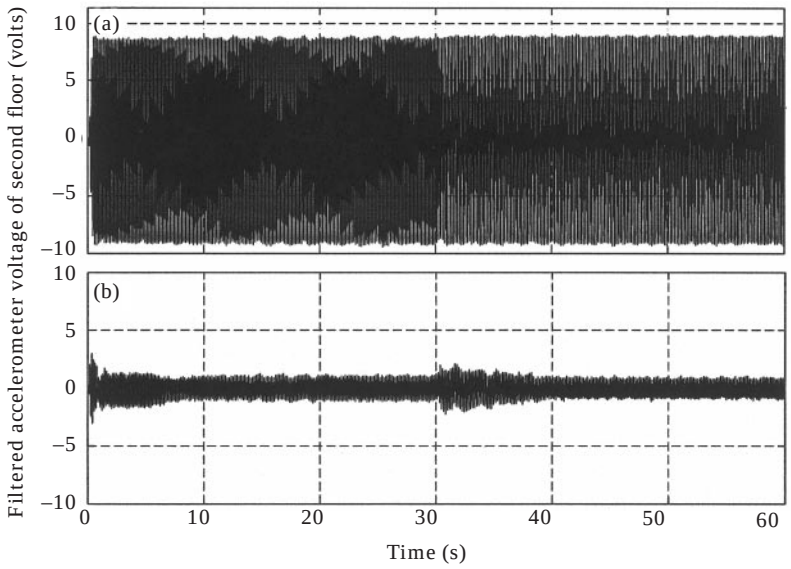

Figure 33. The performance of the adaptive–passive vibration absorber with the second floor as the point of interest: (a) response without vibration absorber appended; (b) response with vibration absorber appended.

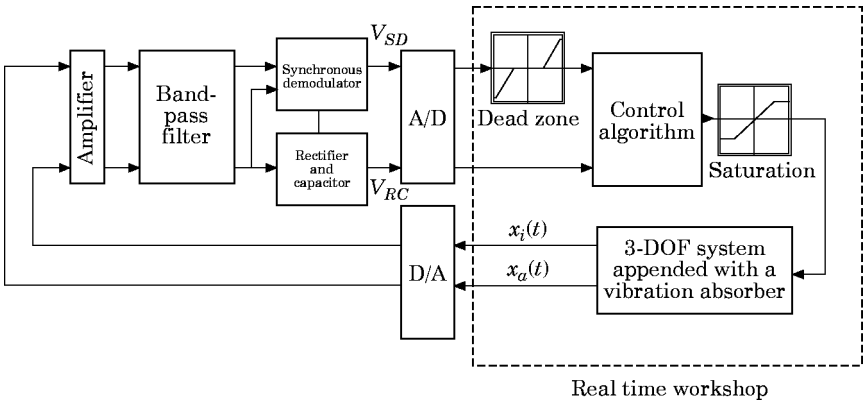

Figure 34. Implementation of the control scheme for simulations.

is illustrated in Figure 33. At steady state the tuned vibration absorber achieves a 18·1 dB and 19·4 dB reduction in the amplitude of filtered accelerometer signal of the second floor for the excitation frequencies of 6 Hz and 5·6 Hz, respectively.

4.4. VIRTUAL SYSTEM APPLICATION

To verify the control algorithm at higher frequencies in order to test other aspects of the controller, a virtual 3-DOF system appended with a vibration absorber will be investigated (Figure 2). This virtual system is built using RTW. Real time simulations of the system are employed so that the controller hardware (amplifier, bandpass filter, rectifier/capacitor circuit and the synchronous demodulator) used in the experimental verification will remain the same. The schematic of this system is shown in Figure 34. The parameters for the virtual system are $M_1 = M_2 = M_3 = 2{\cdot}5$ kg, $C_1 = C_2 = C_3 = 5$ Ns/m, $K_1 = K_2 = K_3 = 10$ kN/m, $m = 0{\cdot}25$ kg and $c = 0$.

4.5. VIRTUAL SYSTEM RESULTS

The simulated results for the 3-DOF system appended with a vibration absorber are separated into two cases. The first case is concerned with vibration attenuation of $x_2(t)$. The second case concerns the attenuation of $x_1(t)$. In each test case, the vibration absorber is initially mistuned. Once the control algorithm has tuned the vibration absorber, the excitation frequency is changed. The control algorithm then retunes the absorber.

4.5.1. *Case* 1: *attenuation of* $|x_2(t)|$

Initially, the excitation is $f(t) = 100 \sin(25{\cdot}25(2\pi)t)$ N. The tuning algorithm is activated at $t = 5$ s. At $t = 50$ s, the excitation is changed to $f(t) = 100 \sin(25(2\pi)t)$ N. The control algorithm parameters ϕ and $\hat{\delta}$ are contingent upon the excitation and system parameters. For this test the parameters are $\phi = 90^\circ$, $\hat{\delta} = 0{\cdot}26$ and $tol = 1{\cdot}2$. The results of the simulation are shown in Figures 35 and 36. The control process for this simulation is shown in Figure 35. Initially the controller is in its first stage of operation. The tuning of the vibration absorber is based on driving the output of the synchronous demodulator, V_{SD} to zero. At approximately $t = 41$ s, the output of the synchronous demodulator is zero. Since the output of the rectifier and capacitor V_{RC} is greater than $\hat{\delta}$, the controller switches to the second stage. In this stage, the controller tunes the absorber spring to increase the spring stiffness. This tuning is based on the feedback error signal developed from the

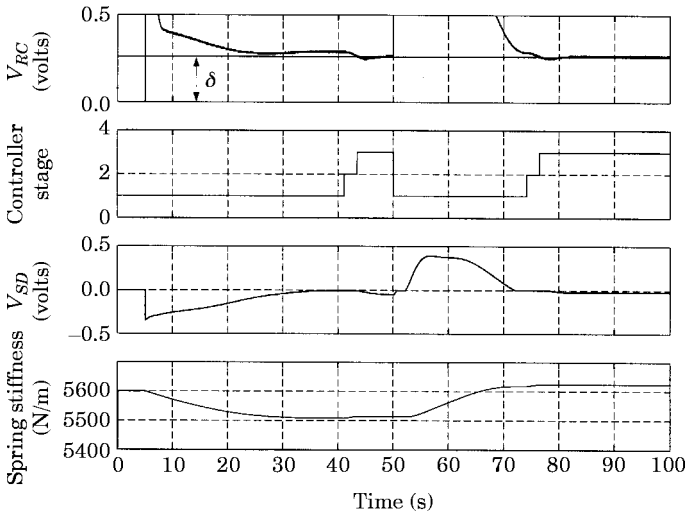

Figure 35. The results of simulation for case 1.

amplitude of V_{RC}. The controller continues to tune spring stiffness until $V_{RC} \leqslant \hat{\delta}$, which occurs at approximately $t = 43$ s. The controller stops tuning and enters stage three. At $t = 50$ s, V_{RC} becomes greater than $(\hat{\delta} * tol)$ as a result of the change in excitation frequency. At this point, the controller begins the stage one tuning process again.

Shown in Figure 36 is the performance of the adaptive–passive vibration absorber with a comparison between the responses for the 3-DOF system with and without the adaptive vibration absorber appended to the structure. At steady state the tuned vibration absorber achieves 6 dB and 5·4 dB reductions in the amplitude of $x_2(t)$ for the excitation frequencies of 25·25 Hz and 25 Hz, respectively.

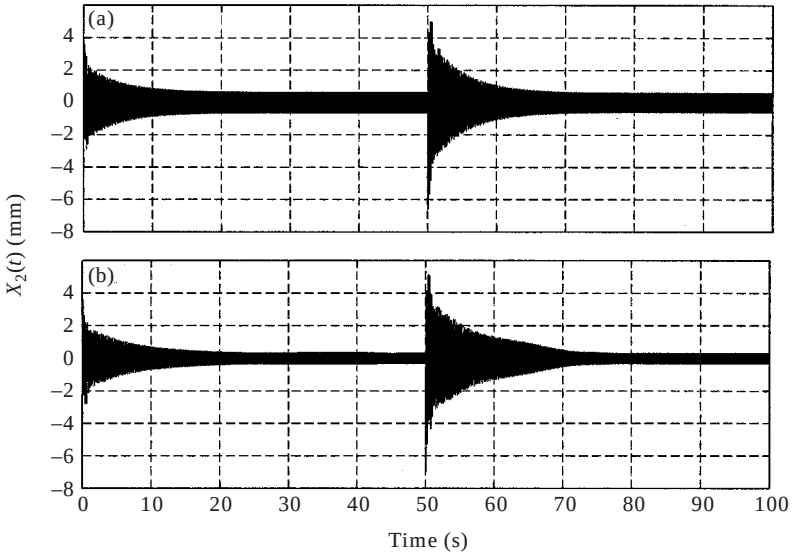

Figure 36. The performance of the adaptive–passive vibration absorber for Case 1: (a) response without vibration absorber appended; (b) response with vibration absorber appended.

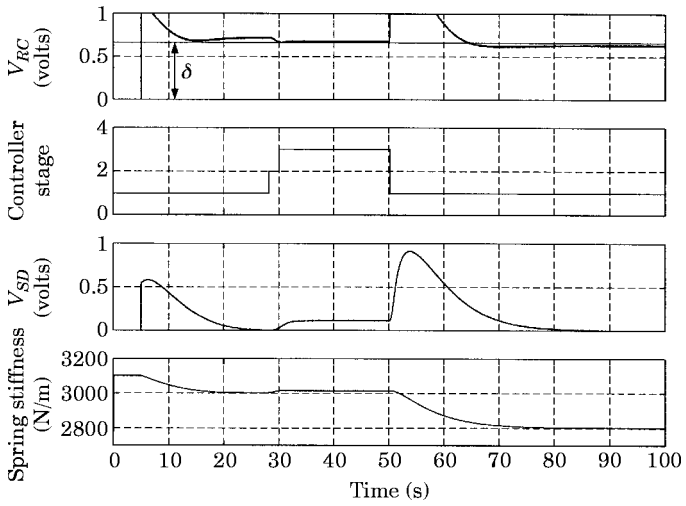

Figure 37. The results of simulation for case 2.

4.5.2. *Case* 2: *attenuation of* $|x_1(t)|$

Initially, the system excitation is $f(t) = 20 \sin (18{\cdot}5(2\pi)t)$ N. The tuning algorithm is turned on at $t = 5$ s. At $t = 50$ s, the excitation is changed to $f(t) = 20 \sin (19(2\pi)t)$ N. For this test, the system parameters are chosen to be $\phi = -90^\circ$, $\hat{\delta} = 0{\cdot}66$ and $tol = 1{\cdot}2$. The results of the simulation are shown in Figures 37 and 38.

The control process for the simulation is shown in Figure 37. Notice that for the final excitation frequency the controller remains in the first stage. Since $V_{RC} \leqslant \hat{\delta}$, the vibration absorber is tuned such that the magnitude is at an acceptable level and the absorber is sufficiently tuned based on the synchronous demodulator output.

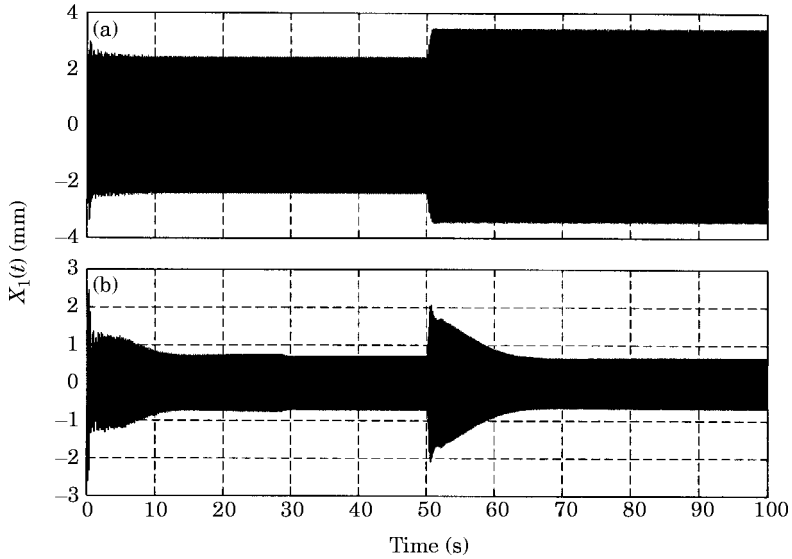

Figure 38. The performance of the adaptive–passive vibration absorber for case 2: (a) response without vibration absorber appended; (b) response with vibration absorber appended.

In Figure 38 is shown the performance of the adaptive–passive vibration absorber, with a comparison between the responses for the 3-DOF system with and without the adaptive vibration absorber appended to the structure. At steady state the tuned vibration absorber achieves 10·6 dB and 14·1 dB reductions in the amplitude of $x_1(t)$ for the excitation frequencies of 18·5 Hz and 19 Hz, respectively.

5. SUMMARY OF ANALYSIS AND EXPERIMENTAL AND SIMULATED RESULTS

The dynamic analysis of a non-collocated passive vibration absorber for vibration attenuation was presented. Performance of the passive vibration absorber is contingent on the amount of damping in the intervening structure–vibration absorber assembly and the relative mass and spring rate of the tuned vibration absorber. It was found that there exists a range of frequencies that cannot be controlled.

Based on the dynamic analysis, a feedback based tuning algorithm for a variable stiffness vibration absorber was developed. First, the feedback tuning algorithm utilizes phase information between the vibration absorber and point of interest to insure a $\pm 90^\circ$ difference. This phase condition results in the absorber being tuned at or near its optimal parameters. The algorithm then uses the amplitude of vibration at the point of interest as a error signal in a feedback regulator structure to minimize the residual vibration to maximize performance.

The experimental and simulated results reveal the effectiveness of the tuning algorithm. In each case, the algorithm is used to reduce the steady state amplitude of vibration at the point of interest through proper tuning of the vibration absorber. Robustness of the algorithm is demonstrated through its ability to robustly adapt to changes in excitation frequency.

ACKNOWLEDGMENT

The authors would like to thank J. William (Bill) Hynd, Senior Design Engineer at PCB Piezotronics Inc., for providing the synchronous demodulator.

REFERENCES

1. M. W. Ryan 1994 *M.Sc. Thesis*, *Purdue University*. Adaptive passive vibration control.
2. R. J. Bernhard, H. R. Hall and J. D. Jones 1992 *Proceedings of Inter-Noise*, *July* 20–22, *Toronto*, *Canada*, 427–430. Adaptive–passive noise control.
3. J. Q. Sun, M. R. Jolly and M. A. Norris 1995 *Transactions of the American Society of Mechanical Engineers* **117**, 234–454. Passive, adaptive and active tuned vibration absorbers—a survey.
4. A. H. von Flotow, A. Beard and D. Bailey 1994 *Proceedings of Noise-Con*, *May* 1–4, *Fort Lauderdale*, *Florida*, 437–454. Adaptive tuned vibration absorbers: tuning laws, tracking agility, sizing, and physical implementations.
5. B. G. Korenev and L. M. Reznikov 1993 *Dynamic Vibration Absorbers*: *Theory and Technical Applications*. New York: John Wiley.
6. W. Bong, Q. Liu and F. Bauer 1993 *Journal of Guidance*, *Control*, *and Dynamics* **16**(6), 1069–1077. Classical and robust H_∞ control redesign for the Hubble Space Telescope.
7. G. J. Balas and J. C. Doyle 1994 *Journal Of Guidance*, *Control*, *and Dynamics* **17**(2), 370–377. Control of lightly damped, flexible modes in the controller crossover region.
8. B. Yang and C. D. Mote Jr. 1992 *Transaction of the American Society of Mechanical Engineers*, *Journal of Dynamic Systems*, *Measurement*, *and Control* **114**(3), 409–415. On time delay in noncollocated control of flexible mechanical systems.
9. T. W. Long, E. L. Hanzevack and S. Caggiano 1995 *IEEE International Symposium on Intelligent Control*, 9–14. Noncollocated vibration control using neural networks.
10. W. R. Evans 1948 *AIEE Transactions* **67**, 547–551. Graphical analysis of control systems.